Variable stiffness corrugated composite structure with shape memory polymer for morphing skin applications

Xiaobo Gong[1], Liwu Liu[2], Fabrizio Scarpa[3,*], Jinsong Leng[1], and Yanju Liu[2,*]

[1]Centre for Composite Materials and Structures, Harbin Institute of Technology, Harbin HIT Science Park, No. 2 YiKuang Street, Harbin, 150080, PR China
[2]Department of Astronautical Science and Mechanics, Harbin Institute of Technology P.O. Box 301, No. 92 West Dazhi Street, Harbin 150001, PR China
[3]Advanced Composites Centre for Innovation and Science, University of Bristol, Bristol BS8 1TR, UK
[*]Authors to whom correspondence should be addressed. Email: yj_liu@hit.edu.cn, f.scarpa@bristol.ac.uk

ABSTRACT

This work presents a variable stiffness corrugated structure based on a Shape Memory Polymer (SMP) composite with corrugated laminates as reinforcement that shows smooth aerodynamic surface, extreme mechanical anisotropy and variable stiffness for potential morphing skin applications. The smart composite corrugated structure shows a low in-plane stiffness to minimize the actuation energy, but also possess high out-of-plane stiffness to transfer the aerodynamic pressure load. The skin provides an external smooth aerodynamic surface because of the one-sided filling with the SMP. Due to variable stiffness of the shape memory polymer the morphing skin exhibits a variable stiffness with a change of temperature, which can help the skin adjust its stiffness according different service environments and also lock the temporary shape without external force. Analytical models related to the transverse and bending stiffness are derived and validated using Finite Element techniques. The stiffness of the morphing skin is further investigated by performing a parametric analysis against the geometry of the corrugation and various sets of SMP fillers. The theoretical and numerical models show a good agreement and demonstrate the potential of this morphing skin concept for morphing aircraft applications. We also perform a feasibility study of the use of this morphing skin in a variable camber morphing wing baseline. The results show that the morphing skin concept exhibits sufficient bending stiffness to withstand the aerodynamic load at low speed (less than 0.3 Ma), while demonstrating a large transverse stiffness variation (up to 191 times) that helps to create a maximum mechanical efficiency of the structure under varying external conditions.

Keywords: morphing aircraft; morphing skin; shape memory polymer; corrugated structure; variable stiffness

1 Introduction

A traditional aircraft configuration is designed around an optimal in-flight cruise operation. At different points of the flight envelope the aircraft does not however perform with the same aerodynamic efficiency. Several different operational segments compose a typical aircraft mission, and aeroplanes are also tasked to accomplish multiple aircraft missions. A morphing aircraft constitutes therefore a suitable platform to accomplish these multi-missions profiles by adapting the aerodynamic and structural shape to extend the aeromechanics flight envelope of the airframe. As the main component to produce aerodynamic forces in classical aircraft designs, the development of a morphing wing is critical to realize the characteristics of a morphing aircraft. Between the different classes of morphing wing designs, one can list the planform alteration concept (span, chord, and sweep changes), the out-of-plane airframe transformation (twist, and span-wise bending), and the airfoil adjustment (camber and thickness) [1-3]. Morphing wing designs have been proposed and evaluated by several research groups, industries and within national/international programmes, like the NASA/DAPPA/AFRL/Next-Gen Inc, FlexSys Inc, teams at Virginia Tech, Universities of Florida, Bristol and Swansea [1-12]. Morphing wings are complex and sophisticated systems, which consist of shape-changing skins, actuators, wing substructures and associated mechanisms [2, 3]. Each component should be designed for a performance trade-off between compliance (i.e., perform the morphed shape), stiffness (to withstand and transfer the aerodynamic loads), and weight (maximize payloads while minimizing the airframe weight) [1, 13]. An additional challenge is fitting the actuation systems for the morphing airframe within a small volume, along with the fuel and other auxiliary units [3]. Aside from the pure structural design, the aerodynamic performance under morphing is subjected to changes, and the development of corresponding control strategies constitute also significant challenges. All the above technological tests make the development of an efficient morphing wing design a difficult task. Despite the difficulties, the advantages of morphing in terms of flexibility and expansion of the flight envelope and mission for an aircraft are attractive for the designers, and morphing flying systems are acknowledged to be a part of future aircraft designs [4].

A morphing skin is an essential part in the design of morphing wings with a smooth aerodynamic surface [6]. A morphing skin should feature a low in-plane stiffness to obtain large deformations and minimize the driving forces, and also possess high out-of-plane stiffness to withstand and transfer in an adequate manner the aerodynamic pressure load. Therefore, the morphing skin should exhibit extreme mechanical anisotropic properties to meet these conflicting requirements [6]. Corrugated sheets possess extreme mechanical anisotropic properties, being flexible in the transverse and stiff in the longitudinal direction. Because of these characteristics corrugated structures have been widely used in the packaging industry and in civil, marine, transport and aerospace structures [14]. Corrugated composite sheets were firstly proposed for flexible wing skins applications by Yokozeki et

al [15]. In that paper the elastic mechanical properties of the corrugations were investigated by using theoretical and experimental analysis. To further increase the anisotropy of the skin and obtain a smooth aerodynamic surface, Yokozeki et al proposed to adopt the use of unidirectional CFRP rods in the valley section and a flexible elastomeric rubber filled on one side. After Yokoseki et al's seminal paper several corrugated structures have been designed and proposed as morphing skins with various geometry and different materials [16-25]. Previtali et al showed the feasibility of using a double-walled corrugated structure to improve the bending anisotropy [26, 27]. A typical corrugation features a series of parallel ridges and furrows [14] that cannot provide a smooth aerodynamic surface. Airfoils with corrugated skins have been extensively studied though experimental and computational aerodynamics, and the results show that the aerodynamic performance is highly dependent upon the corrugation amplitude, the wavelength, the gradient (combination of amplitude and wavelength) and the Reynolds number [28]. The corrugated surfaces generate a larger drag coefficient, provide a detrimental effect on the aerodynamic performance, while low amplitude and low wavelength corrugation provides in general the best performance [28-30]. As well as filling one side of the corrugations with of flexible elastomeric material, several researchers have provided several solutions to produce a smooth aerodynamic surface using structural corrugation platforms. Thill et al have used composite strips bonded to one surface to form a segmented outer skin [31]. Dayyani et al have proposed a composite corrugated core coated with an elastomer as a morphing skin and have explored the mechanical performance of this design from multiple perspectives, including the development of high-fidelity models representing the coated corrugated skin, the nonlinear effects of the elastomeric coating, the deformation mechanisms of the composite corrugated core and the performance of the corrugated skin under buckling loads [22, 25, 32]. Corrugated morphing skins have been so far mainly proposed in camber and chord morphing [31-33], winglet [34] and span wise morphing [18]. The overall results show that the corrugated structures can create a potential morphing to the external airfoil skin at low speeds and for small air vehicles [14, 31].

Several research groups have also investigated the introduction of variable stiffness materials and structures to solve the contradiction between high stiffness and reversible deformability required by morphing structures. The variable stiffness approach to morphing can indeed generate a real time adjustment of the stiffness to create a maximum mechanical efficiency of the structure under varying external conditions [35]. Shape memory polymers (SMPs) undergo substantial stiffness variations when externally stimulated. The most frequent type of stimulation is the thermal activation [36, 37]. SMPs are stiff below their transition temperature, and become flexible and possess large strain capability when heated above that particular temperature. Furthermore, shape memory polymers can harden in a deformed shape as a temporary configuration, a feature that can help morphing skins to be locked into a temporary shape without requiring external forces. Due to their variable stiffness property and their shape memory effect, SMPs had been thoroughly investigated as potential morphing skins in several papers [38-42].

This work presents the design and modelling of a variable stiffness corrugated structure based on the combination SMP and composite corrugated laminates for potential morphing skin applications. The proposed concept exhibits both extreme mechanical anisotropy and variable stiffness. As one-sided filled with of SMP, the skin performs a smooth aerodynamic surface, which help improve the aerodynamics performance of corrugated laminate and lock the temporary shape without external force. Analytical models of the concept related to the transverse and bending stiffness are derived and validated using finite element techniques. Both the transverse and bending stiffness of the corrugated sheet are parametrically investigated versus the geometry of the corrugation. The stiffness of the morphing skin is also globally evaluated versus the variation of the material properties of the shape memory polymer filler to investigate the variable stiffness performance. The theoretical and numerical models show mutual good agreement and demonstrate the feasibility of this morphing skin design. A feasibility study of the performance of this smart skin is performed for a variable camber wing numerical test case using fluid-structure interaction (FSI) involving FE and panel lattice methods.

2 The variable stiffness corrugated structure design and its analytical model

The layout of the variable stiffness corrugated structure is presented in Figure 1. The external skin has a flat surface provided by the SMP filler, which contributes to improve the aerodynamic and the reduction of profile drag of the corrugated laminate.

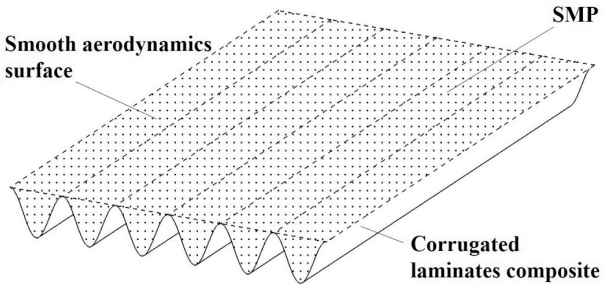

Figure 1 Layout of the variable stiffness corrugated structure design.

2.1 Analytical model of transverse stiffness

The geometry of the corrugation can be described by a sinusoidal curve, its parameters being the amplitude *H/2*, the period *L*, the thickness *t*, and its width *W*. The sinusoidal corrugation is mathematically described as by:

$$y = \frac{1}{2} H sin(\frac{2\pi x}{L}) \quad (1)$$

The analytical model to predict the stiffness is established by using Castigliano's second theorem. The corrugated sheet is considered having a small thickness compared to its planar dimensions. Only the axial and the flexural deformations of the sheet are taken into account, while the shear deformation is neglected [43]. A transverse load is applied to the corrugated configuration, as shown in Figure 2 (a). A segment of the sheet between the origin and a location *x* is isolated and analyzed in Figure 2 (b). When *x=nL/2* and *y=0*, only the horizontal force P (equal to the loaded transverse load) exists. At any other location *x*, the internal force components on the section are constituted by the normal force *N(x)* and the moment *M(x)*, while the shear force *V(x)* is ignored.

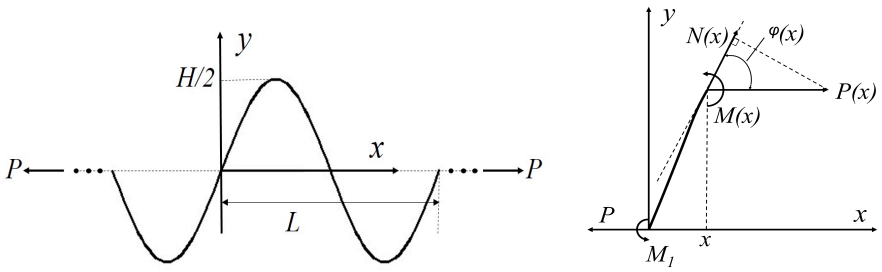

(a) (b)

Figure 2 Forces and moments corresponding to the transverse direction tensile properties: (a) corrugated sheet, (b) arbitrary section of the sheet.

From the equilibrium of forces and moments on the segment of the corrugated sheet the normal force and the moment can be obtained as:

$$N(x) = P\cos\varphi \tag{2}$$

$$M(x) = \frac{1}{2}PH\sin\left(\frac{2\pi x}{L}\right) \tag{3}$$

The deflection in the horizontal direction produced by the transverse load can be derived from Castigliano's second theorem in the case where only the axial and flexural deformations are considered:

$$\delta = \frac{1}{EA}\int N\frac{\partial N}{\partial P}ds + \frac{1}{EI}\int M\frac{\partial M}{\partial P}ds \tag{4}$$

In (4) *E* is the Young's modulus of the core material, *A* and *I* are the area and moment of inertia of the section respectively. The differential of the variable *s*, *ds*, can be expressed as $ds = dx/\cos\varphi$, where $\cos\varphi$ is given by:

$$cos\varphi = \frac{1}{sec\varphi} = \frac{1}{\sqrt{1+tan\varphi^2}} \tag{5}$$

The slope of the corrugation is equal to $tan\varphi$:

$$tan\varphi = \frac{dy}{dx} = \frac{H\pi}{L} cos(\frac{2\pi x}{L}) \tag{6}$$

We consider only half of the sinusoid by symmetry. By substituting expressions (2), (3) and (6) into (4) we obtain:

$$\delta = \frac{P}{EA}\int_0^{\frac{L}{2}} \frac{1}{\sqrt{1+\frac{H^2\pi^2}{L^2}\cos(\frac{2\pi x}{L})^2}} dx + \frac{PH^2}{4EI}\int_0^{\frac{L}{2}} \sin(\frac{2\pi x}{L})^2 \sqrt{1+\frac{H^2\pi^2}{L^2}\cos(\frac{2\pi x}{L})^2} dx \tag{7}$$

The deflection along the horizontal direction produced by the transverse load can be obtained by calculating the integrals:

$$\delta = \frac{PL}{EWt^3\pi^3}((\pi^2t^2 + \pi^2H^2 + L^2)EK\left(\frac{\pi\sqrt{-H^2}}{L}\right) + (\pi^2H^2 - L^2)EE\left(\frac{\pi\sqrt{-H^2}}{L}\right)) \tag{8}$$

In (8) *EK(x)* and *EE(x)* are the first and second kind elliptic integral functions, respectively.

The homogenized linear elastic stress and strain in the corrugated core can be defined as:

$$\begin{cases} \sigma = \frac{P}{(H+t)W} \\ \varepsilon = \frac{2\delta}{L} \end{cases} \tag{9}$$

Therefore, the effective transverse Young's modulus of the corrugated sheet E_x can be expressed as:

$$E_x = \frac{Et^3\pi^3}{2(H+t)}((\pi^2t^2 + \pi^2H^2 + L^2)EK\left(\frac{\pi\sqrt{-H^2}}{L}\right) + (\pi^2H^2 - L^2)EE\left(\frac{\pi\sqrt{-H^2}}{L}\right))^{-1} \tag{10}$$

The transverse stiffness $k = P/2\delta$ can be formulated as:

$$k = \frac{EWt^3\pi^3}{2L}((\pi^2t^2 + \pi^2H^2 + L^2)EK\left(\frac{\pi\sqrt{-H^2}}{L}\right) + (\pi^2H^2 - L^2)EE\left(\frac{\pi\sqrt{-H^2}}{L}\right))^{-1} \tag{11}$$

The transverse stiffness of the plate k_0, made of the same core material with length *L* is:

$$k_0 = \frac{EWt}{L} \tag{12}$$

A dimensionless transverse stiffness can be formulated as:

$$\frac{k}{k_0} = \frac{t^2\pi^8}{2}\left((\pi^2t^2 + \pi^2H^2 + L^2)EK\left(\frac{\pi\sqrt{-H^2}}{L}\right) + (\pi^2H^2 - L^2)EE\left(\frac{\pi\sqrt{-H^2}}{L}\right)\right)^{-1} \tag{13}$$

The SMP fills one side of the corrugation (valley section). The Young's modulus of the SMP is dependent on the temperature, and when considering the significant change of stiffness experienced by the shape memory polymer the analytical model that describes the variable stiffness of the composite is approximated by considering the thermal variation of the Young's modulus of the polymer. When the SMP is heated to a temperature higher than the allowed range limit, its stiffness is significantly smaller than the one of the corrugated laminate, and therefore the SMP can be treated as flexible filler. Similarly to the case of filled honeycombs [44-46], the assumption of the analytical model for the filled composite structure are the following: 1) the valley of the corrugation is entirely packed by the SMP with a uniform distribution, 2) the material behaviour of the SMP matrix is considered linear elastic and isotropic, 3) the matrix is perfectly bonded to the corrugated sheet and 4) the strain distribution in the filler is calculated by considering the corrugated walls as pin-joined mechanisms (shown in Figure 3 (a) as a red dash line). By inspecting the kinematics of the deformation shown in Figure 3 (b), for small in-plane strains the corrugated walls can be assumed to remain straight. The strain in the matrix is therefore uniform and can be calculated as $\varepsilon = 2\delta/L$.

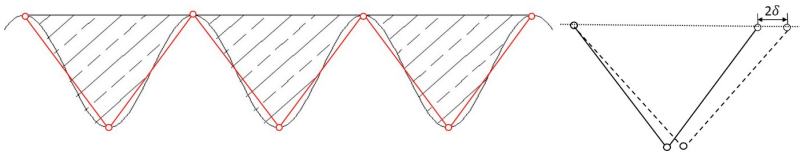

(a) (b)

Figure 3 Approximate analysis of variable stiffness corrugation morphing skin: (a) approximate method, (b) approximated unit of infill.

The additional force caused by the SMP matrix when the corrugated morphing skin undertakes a transverse deformation 2δ can be expressed as:

$$P_i = \frac{E_i WH\delta}{L} \tag{14}$$

The effective transverse stiffness $k_i = P_i/2\delta$ of the SMP filler can be obtained as:

$$k_i = \frac{E_i W H}{2L} \tag{15}$$

By integrating the internal forces in the corrugated sheet and the SMP matrix in a wavelength we can obtain the transverse stiffness of the composite corrugated skin:

$$k_a = \frac{P+P_i}{2\delta} = k + k_i \tag{16}$$

In (16), E_i is the Young's modulus of the shape memory polymer.

2.2 Analytical model of the bending stiffness

The bending stiffness EI is described by the equivalent flexural modulus of the composite E and its second moment of area I. The cross section of the variable stiffness corrugated skin is shown in Figure 4. When we consider one sinusoidal period the bending stiffness of the composite can be expressed as:

$$EI_x = 2E \iint y^2 dA = 2E \int_0^{\frac{L}{2}} \frac{H^2 sin(\frac{2\pi x}{L})^2}{4} t ds \tag{17}$$

In Equation (17) the integrand ds can be replaced by the expression involving dx, which has been derived in the previous section. By performing this substitution and calculating the integral we obtain the bending stiffness of the corrugated sheet:

$$EI_x = \frac{EtL}{6\pi^3}((\pi^2 H^2 + L^2)EK\left(\frac{\pi\sqrt{-H^2}}{L}\right) + (\pi^2 H^2 - L^2)EE\left(\frac{\pi\sqrt{-H^2}}{L}\right)) \tag{18}$$

The bending stiffness EI_{xo} of the equivalent plate with length L made from the same core material is:

$$EI_{xo} = \frac{ELt^3}{12} \tag{19}$$

Also in this case, we can obtain a dimensionless bending stiffness as:

$$\frac{EI_x}{EI_{xo}} = \frac{2}{t^2\pi^3}((\pi^2 H^2 + L^2)EK\left(\frac{\pi\sqrt{-H^2}}{L}\right) + (\pi^2 H^2 - L^2)EE\left(\frac{\pi\sqrt{-H^2}}{L}\right)) \tag{20}$$

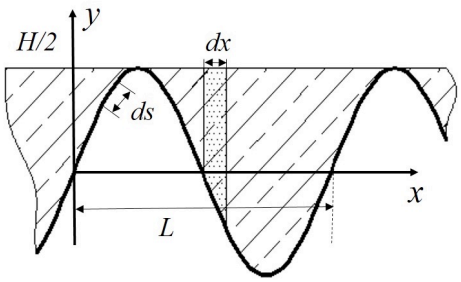

Figure 4 Cross section of the variable stiffness corrugated skin.

To calculate now the bending stiffness of the corrugated composite with the SMP matrix, we need first to calculate the neutral axis of the cross section of the SMP filler:

$$\overline{y_i} = \frac{S_i}{A_i} = \left(\int_{\frac{L}{4}}^{\frac{5L}{4}} dx \int_{y}^{\frac{H}{2}} y\, dy\right) / \left(\int_{\frac{L}{4}}^{\frac{5L}{4}} \left(\frac{H}{2} - y\right) dx\right) = \frac{H}{8} \tag{21}$$

In most practical applications, the corrugated laminate was made with fibre reinforced plastics (FRP) [14, 15, 31], the longitudinal Young's modulus of the corrugated laminate is much higher than that of SMP, especially when the temperature is above the transformation temperature of SMP. So the neutral axis of the cross section of the corrugated skin is assumed to be the *x*-axis, i.e. the same of the pristine corrugated sheet when neglecting the presence of the SMP matrix. The second moment of area for the SMP matrix with regard to the *x*-axis can be expressed as:

$$I_{xi} = \iint y^2 dA = \int_{\frac{L}{4}}^{\frac{5L}{4}} dx \int_{y}^{\frac{H}{2}} y^2 dy = \frac{H^3 L}{24} \tag{22}$$

The bending stiffness of the corrugated skin can be therefore formulated as follows:

$$b_{xa} = EI_x + E_i I_{xi} \tag{23}$$

The corrugated sheet can be made from various substrates, ranging from metals to composite materials like woven or unidirectional carbon/glass epoxy [14, 15, 31]. The elastic constants of the composite laminate can be obtained using classical laminate theory (*[A]*, *[B]*, and *[D]* matrices) [47]. The stiffness EA and EI can be replaced by the terms WA_{11} and WD_{11} respectively in Equation (4), and the Young's modulus E can be replaced by the membrane term A_{22}/t in Equation (17), where A_{11}, D_{11}, A_{22} are corresponding entries in *[A]* and *[D]* matrices [47]. The corresponding transverse and bending stiffness of the composite laminate can be obtained by simple mathematical manipulation.

3 Finite element modelling

To validate the analytical models related to the transverse and bending stiffness of the corrugated composite structures we have performed numerical simulations using a commercial FE (Finite Element) code (ANSYS, version 15.0, Ansys Inc.). Two specific types of elements have been used, SHELL181 for the corrugated sheet and SOLID185 for the SMP matrix. The interface between the corrugated sheet and the SMP was meshed by bonded contact pairs (TARGET170 for the corrugated shells and CONTACT174 for the shape memory polymer filler). Due to the application of the bonded contact pair, no sliding or separation between faces is allowed, which supports the simulation of a perfect bond constraint. After a convergence test the mesh density was fixed at 100 elements per line of geometric wireframe. The Finite element model of corrugated composite and contact pair between corrugated laminate and SMP used to calculate the equivalent transverse stiffness were demonstrated in Figure 5. Two types of parametric simulations were performed to investigate the extreme mechanical anisotropy and variable stiffness. As for the extreme mechanical anisotropy of corrugated sheet, the geometric configurations used in the numerical models have a period $L = 10mm$, thickness ratios $t/L = 0.1, 0.05, 0.02$ and 0.01 and corrugation ratios H/L ranging between 0.1 and 1 with a step of 0.05. In these FE models the corrugations are made with ($E = 200\ GPa$ and Poisson's ratio $\nu = 0.3$). As for the variable stiffness of corrugated composite with SMP, the property of SMP is involved in the FE model. The temperature-dependent mechanical properties of the SMP have been entered via a table. The temperature ranges between 20°C and 150°C with a step 2°C. The geometric configurations are the same with corrugated sheet except the thickness ratio. The thickness ratio is set as a constant determined by thickness of carbon fibre prepreg and number of layers. In this part the corrugated sheet is treated as composite laminate, the material properties of carbon fibre prepreg T300/epoxy are listed as follows: $E_{11} = 137.47GPa, E_{22} = 10.07GPa, G_{12} = 7.17GPa, \vartheta_{12} = 0.23, thickness = 0.125mm$. Corrugated composite laminates with the stacking sequence of [0,90,0] are simulated in FE analysis. The SMP discussed in this work was an epoxy-based thermoset consisting three parts, the epoxy resin, the curing agent, and a linear monomer [48]. The material property of SMP infill is temperature dependent; its elasticity can be investigated by DMA (Dynamic Mechanic Analysis) test. The DMA was conducted using a dynamic mechanical analyzer (Mettler-Toledo AG Analytical, Switzerland). The specimen with dimensions of 9.0x3.0x1.0mm^3 was performed in three-point bending mode at a constant heating rate of 5 °C·min^{-1} and an oscillation frequency of 1 Hz from room temperature 22 °C to 150 °C. The curves of the storage modulus and the tanδ versus the temperature for the SMP are plotted in Figure 6. The relationship between the storage modulus and the temperature can be expressed by a power function as follows:

$$E = a_1 e^{-\left(\frac{T-b_1}{c_1}\right)^2} + a_2 e^{-\left(\frac{T-b_2}{c_2}\right)^2} \quad (24)$$

Where a_1=715.5, b_1=15.66, c_1 =14.16; a_2=1359, b_2 =37.54 and c_2=30.49. The goodness of fit R^2= 0.99.

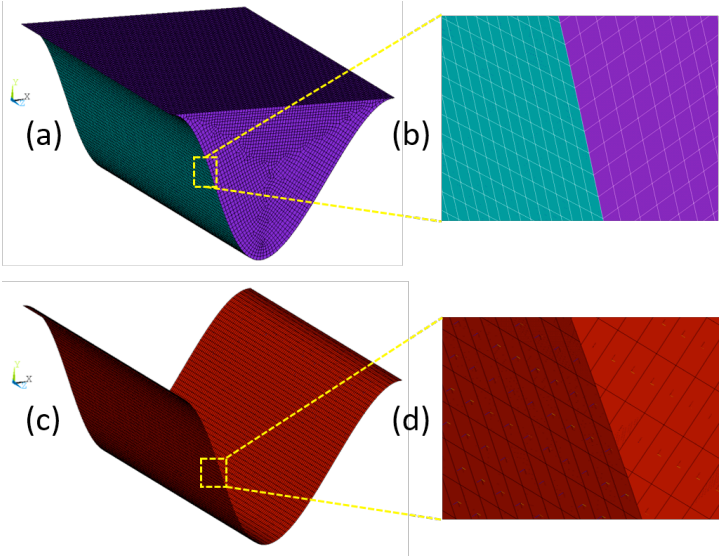

Figure 5 Finite element model of corrugated composite and contact pair between corrugated laminate and SMP used to calculate the equivalent transverse stiffness: (a) and (b) are finite element model and its zoom in, the blue surface is composite laminate the pink solid is SMP; (c) and (d) are contact pairs and its zoom in.

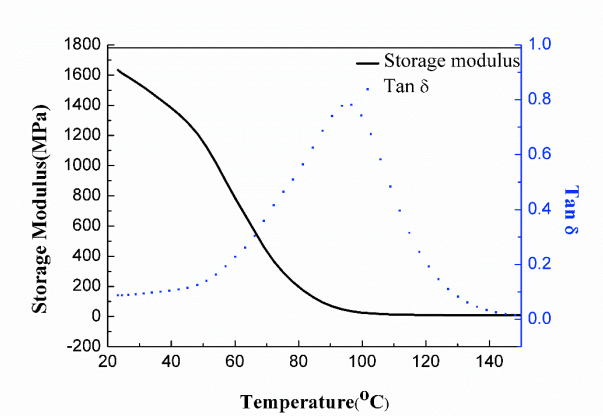

Figure 6 Storage modulus and tanδ versus the temperature of the SMP.

The FE models take advantage of the symmetry of the structure, and therefore one sinusoidal period only is considered as the representative volume element (RVE). The widths of the RVEs, W, are 10mm and 120mm for the simulations of the transverse and bending stiffness, respectively. The transverse stiffness is calculated from the simulation of a transverse tensile load, while the flexural stiffness is obtained by a three points bending test. The boundaries and their conditions are shown in Figure 7 and Table 1, respectively. In the transverse stiffness analysis, the nodes on line B had symmetric boundary. The transvers stiffness can be obtained as the ratio between the reaction forces

and the imposed displacement. For the analysis related to the bending transverse stiffness the nodes lying on the lines A and B and on the surface C have symmetric boundary conditions. The bending stiffness can be derived by using the standard beam theory for cantilever beams [49]. The middle span deflection can be expressed as $\omega = (Fl^3)/48EI$ and the bending stiffness is therefore obtained as:

$$EI = \frac{2F(2L)^3}{48u_2} = \frac{FL^3}{3u_2} \tag{25}$$

Where F is the reaction force at the boundary C along the 2-direction.

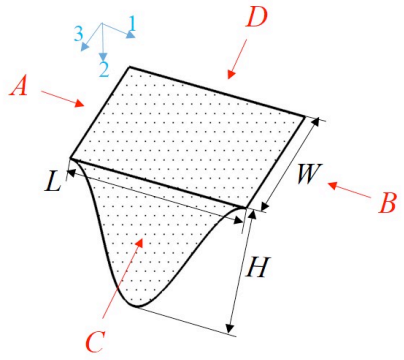

Figure 7 Finite element models of variable stiffness corrugated skin

Table 1 Boundary conditions applied to the FE models to calculate the engineering constants

Boundary	Transverse stiffness	Bend stiffness
A	$u_1 = u_2 = u_3 = 0$ $rot_1 = rot_2 = rot_3 = 0$	$u_1 = rot_2 = rot_3 = 0$
B	$u_1 = imposed$ $rot_2 = rot_3 = 0$	$u_1 = rot_2 = rot_3 = 0$
C	Free	$u_2 = imposed, u_3 = 0$ $rot_1 = rot_2 = 0$
D	Free	$u_1 = u_2 = u_3 = 0$ $rot_1 = rot_2 = rot_3 = 0$

4 Results and discussions

4.1 Anisotropic properties

The relative transverse stiffness vs. the corrugation ratio is shown in Figure 8. The relation between the relative transverse stiffness and the corrugation ratio is remarkably nonlinear, with a decrease at higher corrugation ratios *H/L*, but also featuring an increase for augmenting values of the thickness ratio *t/L*. The corrugated sheet tends to provide higher bending deformation for increasing

corrugation ratio and decreasing thickness ratios. The bending deformations of the corrugated sheet result in larger transverse displacement, and therefore lead to a lower relative transverse stiffness. The relative transverse stiffness obtained by using the FE models shows a very close agreement with the theoretical predictions. The theoretical predictions show an average relative error with the FE results equal to 3.3% on average. The results from the FE analysis tend to be slightly higher compared to the ones from the theoretical investigation. The FE model uses SHELL 181 elements based on Mindlin plate theory that considers the transverse shear deformations, however the theoretical analysis is based on adopting simplified Euler-Bernoulli beams that neglect the transverse shear strains. By ignoring these transverse shears, the theoretical model produces a smaller deformation that results in a higher transverse stiffness. However, the corrugated sheet can be treated as a thin shell, therefore the simplification used in developing the theoretical model is sound. The transverse stiffness of corrugation sheet is 3.8e-5 times lower than the one of the equivalent plate made from the same core material, and therefore the corrugated structure shows the required low in-plane stiffness to yield large deformations and minimize actuating forces.

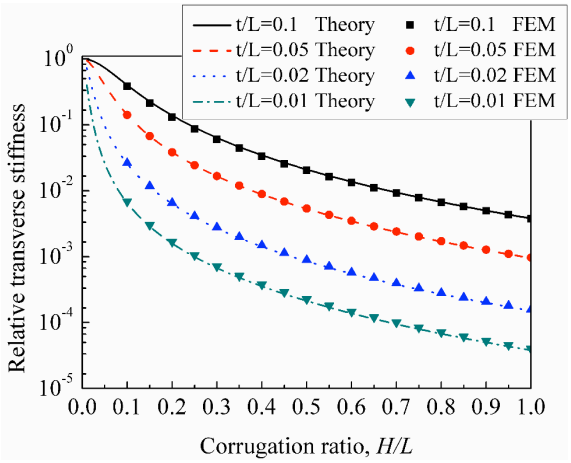

Figure 8 Relative transverse stiffness vs. corrugation ratio for different thickness ratio.

Figure 9 shows the relative bending stiffness vs. the corrugation ratio for different thickness ratios. Similarly to the relative transverse stiffness, the relation between the relative bending rigidity and the corrugation ratio is nonlinear. The bend stiffness increases with increasing corrugation ratio *H/L*, but decreases for increasing values of thickness ratio *t/L*. The relative transverse stiffness obtained by using the FE techniques shows a very close agreement to the theoretical prediction, except for configurations related to low corrugation and high thickness ratios. When the height is comparable with thickness the simplification adopted in equation (17) ($dA = tds$) is not more valid and the relative error is large. In practical applications the height will be larger than the thickness, so the theoretical model provides a reasonable accuracy, with an average relative error of 2.1%. The bending stiffness of the corrugated sheet is 2.6e4 times higher than the one of the equivalent plate made from

the same core material, and therefore the corrugated structure possesses the high out-of-plane stiffness necessary to withstand the aerodynamic pressure load.

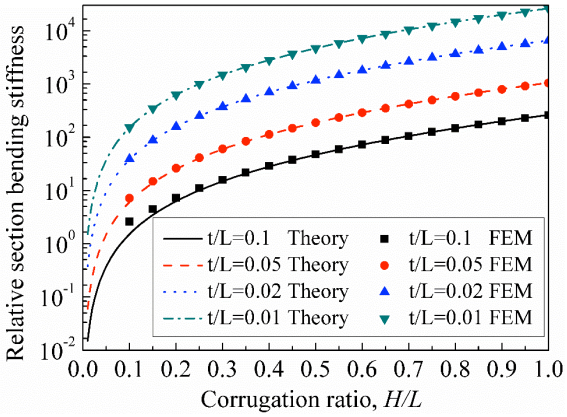

Figure 9 Relative bending stiffness vs. corrugation ratio for different thickness ratios.

4.2 Variable stiffness property

The transverse and bending stiffness of the morphing skin with the shape memory polymer at different temperatures are shown in Figures 10 and 11, respectively. Similarly to the Young's modulus of the pristine SMP, the morphing skin is stiff at low temperatures, and becomes flexible within hotter environments. When the temperature is higher than the SMP transition temperature, both stiffnesses drop to values similar to the ones of the corrugated laminate without the SMP filler. The shape memory matrix does not produce however extra stiffness requiring extra actuation energy at high temperatures, but it contributes to the surface finish for the aerodynamic external flow. The variations of stiffness increase with the increase of the corrugation ratio. When the corrugated laminate has a constant period length *L,* the fraction of the SMP filler increases for increasing corrugation ratios. It is also apparent that the transverse stiffness is subjected to larger variations and demonstrates more evident variable stiffness properties compared to the bending one. The transverse stiffness varies 575 times between 20°C and 150°C, while the bending stiffness is only modified 1.1 times within the same temperature range. As the Young's modulus of the composite corrugated laminate E_{22} is much higher than the one of the SMP the bending stiffness of the morphing skin is only marginally influenced by the variable Young's modulus of the SMP filler. It is also worth noticing that, besides the variable stiffness, the shape memory polymer possesses as well as shape memory effect, which can lead the morphing skin to freeze the deformed shape as a temporary configuration and locks the temporary shape without the use of an external force [35, 42].

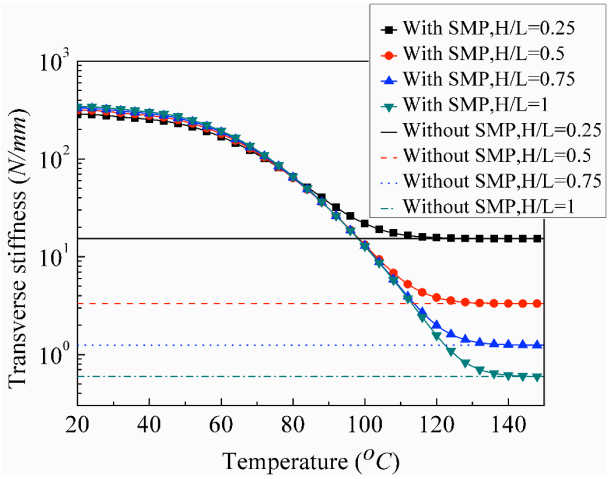

Figure 10 Transverse stiffness vs. the corrugation ratio

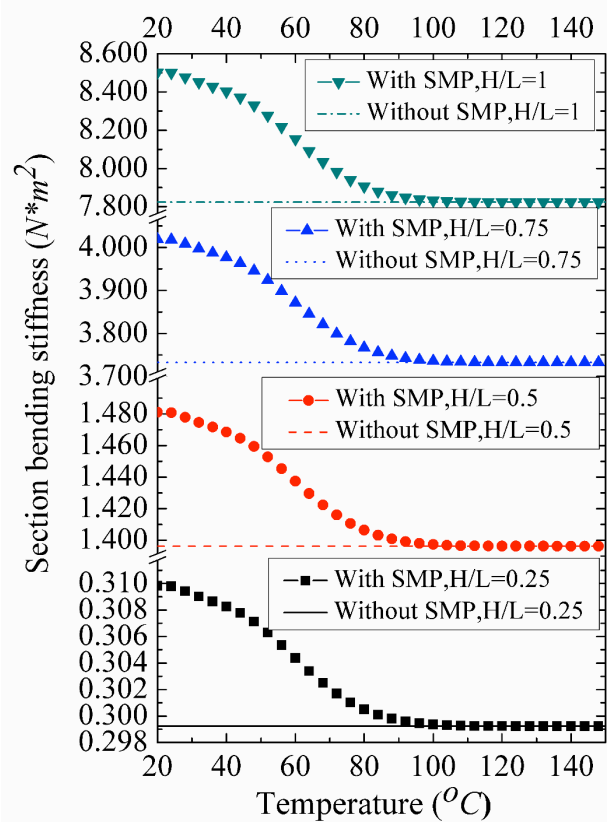

Figure 11 Section bending stiffness vs. the corrugation ratio

Weight is an important part of the assessment of the performance of a morphing skin. Figure 12 shows the variation of weight ratios vs. corrugation ratio. In our case we consider two definitions of weight ratio: one as the ratio between the corrugated composite skin with the SMP filler versus the one of an aluminum alloy skin with the same bending stiffness of the cross section (W_{ms}/W_{Al}); the second is the ratio between the weight of the corrugated composite skin with the SMP filler versus the pure corrugated composite laminate (W_{ms}/W_C). For these simulations we consider two corrugated composite laminates with stacking sequences of [0,90,0] and [0,0,90,0,0]. The mechanical properties

are presented in Finite Element modeling section, while the density for the SMP polymer is considered as 1.58 g/cm^3. The material properties of the aluminum alloy consist in a Young's modulus of 71GPa, Poisson's ratio of 0.33 and density of 2.77 g/cm^3. It is possible to observe that the weight ratios increase with the increase of the corrugation ratios. When the corrugated laminate has a constant period length L, the fraction of the SMP filler increases for increasing corrugation ratios. By taking advantage of the corrugation structure and the high specific modulus of the composite, the corrugated composite skin is lighter by around 50% the weight of the aluminum alloy skin with the same bending stiffness. The corrugated SMP composite skin is however twice as heavy as the pure corrugated composite laminate.

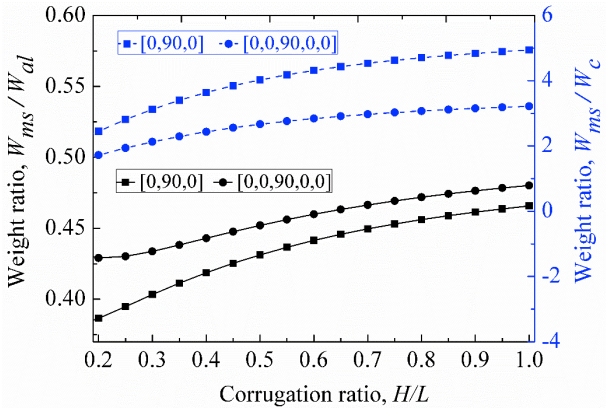

Figure 12 Weight ratios vs. the corrugation ratio

The comparison between the finite element and the analytical models for the tensile and bending stiffnesses are shown in Figure 13. The bending stiffness of the morphing skin structure simulated by the FE and analytical model shows a significant agreement. The tensile stiffness obtained by using the two models shows however agreement only at high temperatures, and some significant discrepancies at low temperatures. The analytical model for tensile stiffness was based on the assumption that SMP can be treated as flexible filler when it is heated to a temperature higher than the allowed range limit, as state in section 2.1. However, those assumptions are invalid at low temperature, the two models show some significant discrepancies. The average error between models is about 1.7% for the bending stiffness, and the maximum one for the tensile stiffness is 375%. The analytical model for tensile stiffness can therefore be used to obtain approximate values at high temperatures and low Young's modulus of the SMP, but a modified model appears to be necessary for more accurate estimations.

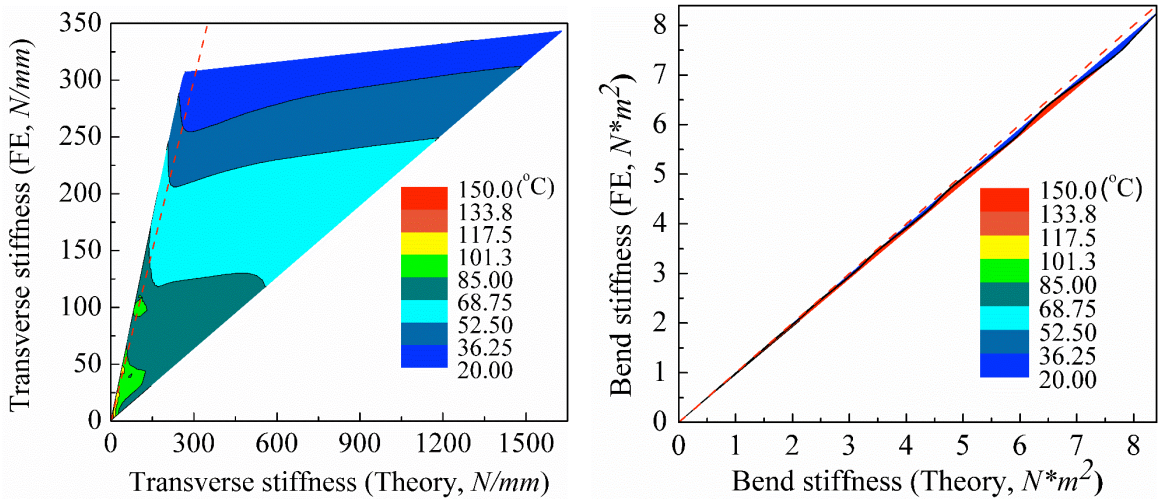

(a) (b)

Figure 13 Comparison between the finite element and the analytical models: (a) tensile stiffness, (b) bend stiffness.

Because of the significant change of stiffness generated by the SMP, the analytical model of the variable stiffness structure can be established for different stiffness ranges. A surface response method (SRM) has been therefore setup to provide a general design tool for the SMP corrugated morphing skin. The SRM has been established from the entire data set acquired through the FE and the analytical models at 1254 different configurations, with stiffness ranges limited to the ratio between the effective transverse stiffness of SMP filler and the corrugated laminate up to 3. When the stiffness ratio is lower than that value, the analytical model shows significant agreement with the FE model, (Figure 14), and the average error is about 1.8%. At stiffness ratios higher than 3 the transverse stiffness of the morphing skin can be approximate by linking directly the temperature with the effective transverse stiffness of the corrugated laminate and the SMP filler as:

$$k_a = k + \mathrm{f}(\gamma,\mathrm{T})k_i \tag{26}$$

The relation $\mathrm{f}(\gamma,\mathrm{T})$ is obtained by a least squares fitting (R^2=0.98 and 95% confidence level) over 789 configurations, the data set and fitting surface being shown in Figure 15:

$$\mathrm{f}(\gamma,\mathrm{T}) = p_1\gamma^3 + p_2T^3 + p_3\gamma^2 + p_4T^2 + p_5\gamma + p_6 \tag{27}$$

In equation (27), γ is the corrugation ratio, T is the temperature, and the coefficients are p_1=-1.277, p_2=8.882e-7, p_3=3.237, p_4=-3.966e-5, p_5=-3.115 and p_6=1.32.

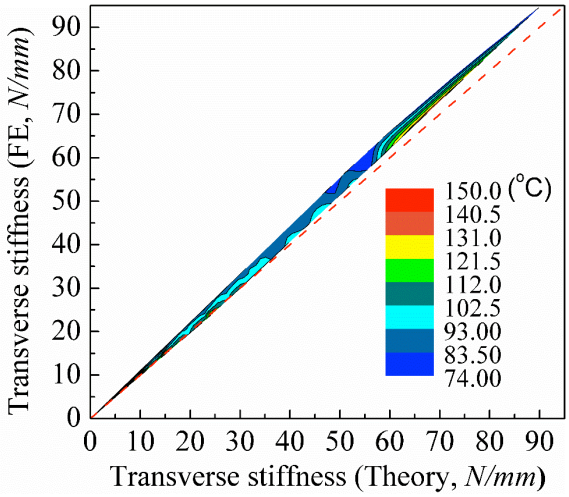

Figure 14 Comparison between the finite element and the analytical model for the tensile stiffness within the stiffness range considered for the SRM

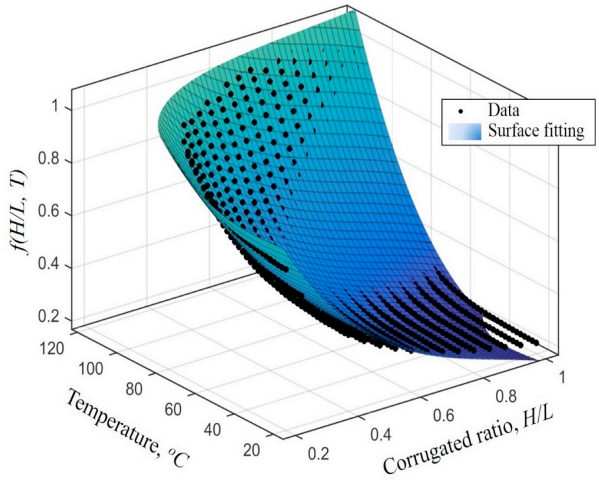

Figure 15 Tensile stiffness of the finite element model and surface fitting beyond the stiffness range

5 Performance of a variable camber wing skin

The preliminary evaluation of the smart composite corrugated skin structure is performed on a model representing the upper skin of a variable camber wing concept, which consists of a corrugated morphing skin, leading and trailing edges, and compliant ribs (Figure 16a). The geometry, aerodynamic and environmental parameters defining the wing configuration are listed in Table 2. We consider a NACA 0012 wing section characterized by a rigid D-spar leading edge, which is structure commonly used to carry global loads [50], and it is widely used in several UAV morphology evaluations [6, 13]. The chord dimensions used (500 mm) are also compatible with the ones existing in current UAV wings and helicopter blades (250 mm – 800 mm). The hollow D-spar leading edge occupies 25% chord, the rigid trailing edge occupies 21% of the chord; both stretch the entire wing

span along a rectangular platform. The rigid parts can be fabricated by aluminium alloy or composites, and thickness depends on the material properties. For the purpose of the skin evaluation only the upper composite corrugated structure/SMP filler is represented with simply supported boundary conditions along the edges of the chordwise direction of the skin, and clamped conditions on the upper and lower sides along the span. The clamps correspond to the regions of the skin attached to the D-spar and to the section of the trailing edge. The composite corrugates part is considered being made by carbon fibre T300/914 epoxy (density 1.58 g cm^{-3}, E_1 = 73.5 GPa, E_2 = 63 GPa, ν_{12} = 0.055, ν_{21} = 0.036). The SMP used in these simulations has the same mechanical properties described in paragraph 3, with a density of 1.18 g cm^{-3}. In the ideal representation of this morphing wingbox, the aerodynamic pressure on the morphing skin and the trailing edge can be transferred to the compliant ribs and to the leading edge, which is the main load bearing entity. Because the feasibility study focuses however on the performance of the corrugated smart morphing skin only, the particular morphology of the actuator and mechanical performance of the leading and trailing edges and the compliant ribs are not described, although the interested reader can find related information in previous works [1, 6, 10]. The simplified representation of Figure 16b may lead to overly conservative results because it does not take into account the base flexibility provided by the D-spar and the trailing edge. For the purpose of this evaluation however, the results could be used to benchmark the actuation authority and performance of the skin versus other smart materials available in open literature [57].

The deflection and actuation force requirements of the morphing skin at different loading conditions have been investigated using a FE code code (ANSYS, version 15.0, Ansys Inc.). The large changes in aerodynamic pressure during morphing have required the use of a sequential coupled fluid/structure-interaction analysis for the determination of the static equilibrium [51]. The airfoil shape is built by overlaying the thickness distribution [52] for the NACA 0012 airfoil onto a parametrically defined camber line. The camber line of the morphing segment of the airfoil is defined from a third order polynomial shape function, which is suited to describe the shape of the variable camber morphing wing that relies on compliance or bending of the internal structure [53]. The method for a parametrically defined airfoil shape has been described in detail by Woods et al [53]. The trailing edge deflection (TD) was set as 5% and 10% of the chord length. The morphing airfoil shapes are shown in Figure 17. The aerodynamic pressures were obtained by using the XFOIL lattice panel-method code, which provides correlated aerodynamic performance predictions with high-fidelity computational fluid dynamics simulations for the types of smoothly cambered deflected shapes [51]. To improve prediction accuracy, a viscous boundary layer component was involved in XFOIL. The boundary layer was described by a two-equation lagged dissipation integral boundary layer formulation with an en transition model [54] (n was set as 9 here according the XFOIL user guide). The distribution of the pressure coefficient over the different airfoil shapes under different freestream velocities is shown in Figure 17. The distribution of the pressure coefficient is dominated by the

airfoil shape, the larger camber of chord the bigger absolute value of pressure coefficient, which means (predictably) that the lift performance can be improved by increasing the camber of the chord efficiently. The resulting aerodynamic pressure P at sea level on the skin surface can then be calculated from the pressure coefficient. The upper skin carries higher suction loads (indicated by larger magnitude negative C_p). The FE model representing the upper part of the wing section with the upper morphing skin was used to verify the stiffness performance of the corrugated smart composite.

As actuation mechanism for the SMP part of the corrugated skin Joule resistive heating could be considered in conjunction with electrically conductive materials. Corrugations made form continuous carbon fibres and carbon fibre felt adhesive on the corrugated composite laminates are considered as promising methods for morphing skin application [37, 55].

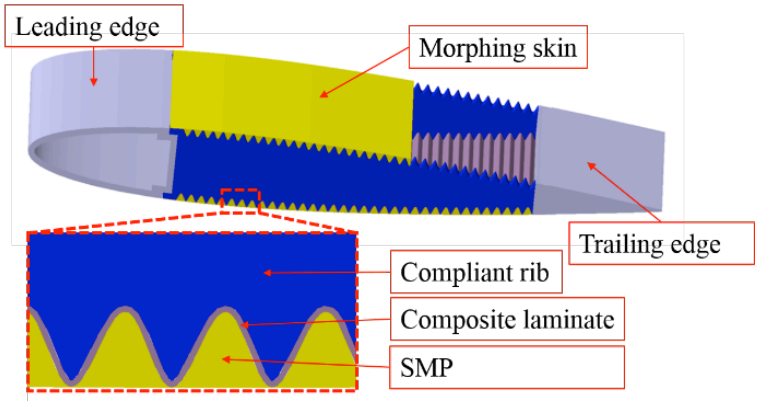

(a)

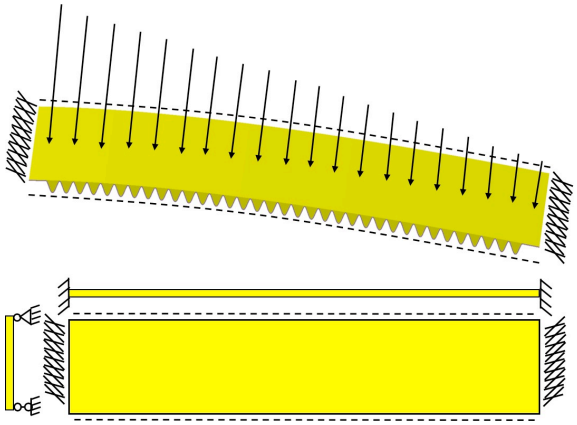

(b)

Figure 16 (a) Variable camber wing concept with the smart composite corrugated structure. (b) simplified model taking into account the skin only and the aerodynamic loading.

Table 2 Geometrical and analysis parameters

Parameter	Value	Units
Baseline airfoil	NACA 0012	n/a
Span, W	200	mm

Chord, C	500	mm
Morphing start	25% C	n/a
Morphing segment	56% C	n/a
Max Trailing edge deflection, TD	[0, 0.05C,0.1C]	mm
Angle of attack, α	5	degrees
Freestream velocity, V	[0.03:0.1:0.3]	Ma
Temperature, T	[20:10:150]	°C
Reynolds number, Re	$\mathrm{Re} = {}^{\rho VC}/_{\mu}$, $\rho = 1.229\ \mathrm{kg}/m^3$, $\mu = 1.73E-5\ P \cdot s$	n/a

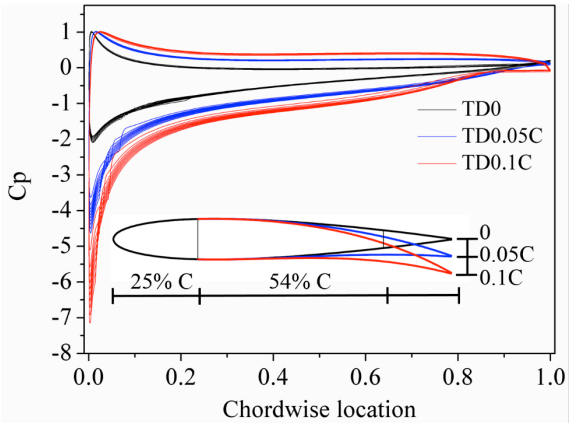

Figure 17 Distribution of pressure coefficient over the different airfoil shape surface under different freestream velocities from XFOIL. The airfoil shapes depend on the trailing edge (TD) percentage variations versus the camber (C) at 0 % (0), 5 % (0.05C) and 10 % (0.1C)

The distribution of the pressure coefficient over the airfoil surface obtained from XFOIL was applied of the FE model to generate the deflection of the morphing skin. The FE model used consists of 34 representative volume elements (RVE), as shown in Figure 18. The geometrical parameters have amplitude of 3 mm, period of 8 mm, and width of 200 mm. The corrugated composite laminates with stacking sequences of [0/90/0] are simulated with shell elements (thickness of 0.375mm). The elements and material properties are the same as the one used in section 3. The morphing skin is fixed on the leading and trailing edges, and supported by the compliant ribs. The boundary conditions applied to the FE models are fixed constraints at the boundaries A and B, with blocked deformations along the direction 3 of boundary D. The FE models take advantage of the symmetry of the structure, (1/2 width, and symmetric constraints on boundary C). The aerodynamic pressure from XFOIL was applied on the top surface of the morphing skin.

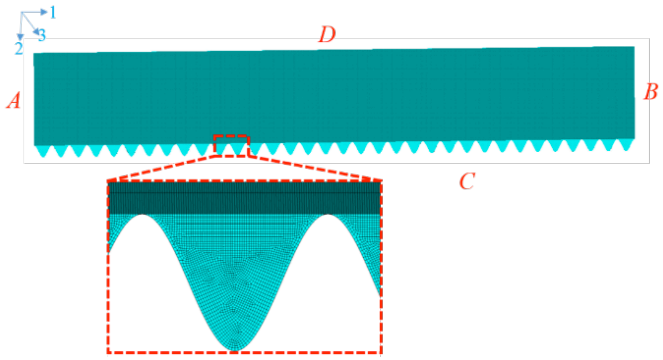

Figure 18 Finite element model of the smart composite corrugated skin

Figure 19 shows the distribution of the deflections on the upper skin for α=5°, V=0.3Ma, T=120 °C, TD=0.1C. The normal deflection field correlates with the aerodynamic pressure distribution, with the maximum deflection occurring at the location of the plane of symmetry close to the leading edge. The maximum deflection of the upper skin for different conditions (α=5°, V=0.03-0.3Ma, T=20-150 °C, TD=0, 0.05C and 0.1C.) are shown in Figure 20. The maximum deflection obviously increases with the increasing velocity, trailing edge initial deflection and temperature. The stiffness of the morphing skin decreases with increasing temperature, based on the variable stiffness of the SMP. The increasing pressure load and decreasing stiffness results in an increase of the maximum deflection, which is very significant when the temperature is over 140 °C. The highest deflection value of 1.87 mm is observed for TD0.1C at 150 °C. The SMP filler goes into rubber state at significantly higher temperatures than at its transition temperature. As a result the deformation of the SMP matrix becomes the dominant parts of the deflection of the morphing skin, and the corrugated composite laminate is not able to constraint the deflection at an acceptable value. The maximum deflections at 140 °C at a location of 0.001 C are however smaller than 0.5mm (0.001C). According the results obtained by Jacobs [56], the drag of the airfoil increases only slightly when the skin deflection does not exceed the 0.1% of the chord. The smart composite corrugated structures appear to provide sufficient stiffness to withstand the aerodynamic load at low velocities (less than 0.3 Ma) when activated below 140 °C.

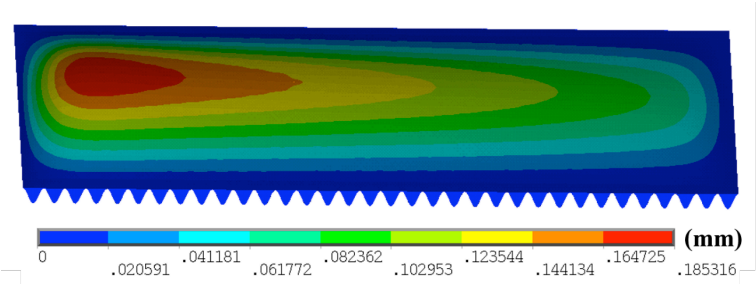

Figure 19 The deflection distribution on the upper morphing skin for α=5°, V=0.3Ma, T=120 °C, TD=0.1C

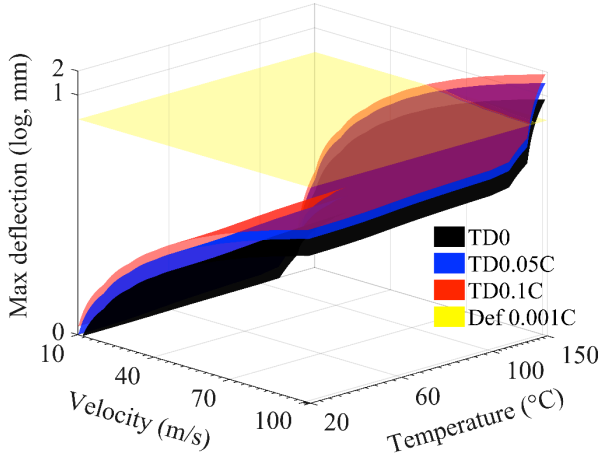

Figure 20 The maximum deflection of the upper morphing skin under different conditions (α=5°, V=0.03-0.3Ma, T=20-150 °C, TD=0, 0.05C and 0.1C.)

Another quantity evaluated during this feasibility study is the actuation force. The morphing skin is highly compliant above the SMP transition temperature, a fact that helps to reduce the actuation force requirements. To provide a change of the variable camber from 5% to 10% of the trailing edge the upper skin should undergo tensile strains between 1.6% and 4.1%. The actuation forces for two values of strains have been numerically computed using the same boundary conditions A, C and D of the previous simulations. The displacements along the 1-direction were 4.29 mm and 11.29 mm, respectively. The displacement vector sum on the upper morphing skin is shown in Figure 21. The displacement increases uniformly along the chord, while remaining almost constant along the span. As the normal deflection field correlates with the aerodynamic pressure distribution (Figure 19), the ununiform displacement occurs at the location of the plane of symmetry close to the leading edge. Figure 22 shows the behavior of actuation force per unit volume of the skin (F/V) and the specific actuation stress σ/ρ at different temperatures. In this case F is the reaction force at the boundary B, σ is the homogenized linear elastic stress (Equation 9), V is the volume of the SMP fill ($V=163.2\ cm^3$) and ρ is the density of the SMP/carbon corrugated structure ($\rho=1.256\ kg/m^3$). The specific actuation force decreases dramatically with the increasing temperature, dropping from 36.4 MN/m^3 and 95.8 MN/m^3 to 0.19 MN/m^3 and 0.50 MN/m^3 within the 20-140 °C. The stiffness of the morphing skin varies 191 times. Compared with the performance characteristics of the actuator listed by Huber et al [57], the maximum specific actuation stress occurring at 20 °C is lower than the one featured by shape memory alloys, hydraulic and magnetostrictive actuators. The minimum specific actuation stress at 140 °C is also lower than the one of pneumatic, muscle and piezoelectric actuators. The variable stiffness of the SMP skin contributes does contribute to a real time adjustment of the stiffness to offset varying external conditions. However, when the temperature is higher than the SMP transition the shape memory matrix does not produce the extra stiffness required for to extra actuation energy, but

only contributes to maintain a surface finish for the aerodynamic external flow. At temperatures lower than the SMP transition the matrix significantly enhances the overall stiffness of the corrugated composite.

The analysis carried out so far does not include any failure or debonding between the matrix and the skin, and the effects of brittleness of the SMP at temperatures below the SMP transition (which would affect the structural integrity of the skin under bending and torsion loads) are not taken into account. From the operational and systems perspective, it is worth mentioning that the use of shape memory polymers in a morphing skin is also prone to be subjected to severe constraints. Heating the polymer is a uniform or local distribution involves a specific design of distributed heaters with complex distributions and with an additional burden to the power budget of the aircraft. The uniform heating is also a condition not necessarily met because of the intrinsic difficulties related to the thermal conduction through the polymer. The exposure of the SMP to UV and solar radiation is also a factor that affects the cross-linking of the polymer, and therefore its mechanical performance and structural integrity, also from a fatigue life point of view. Operational conditions like rain, hail and local convective phenomena do also affect the performance of the polymer, especially its erosion shield properties. Local thermal gradients and the external airflow can also affect the performance of the heating process, therefore decreasing the whole actuation authority of the system. Compared to the pure corrugated composite skin, the additional use of the SMP implies a weight penalty. While the latter can be minimized by replacing the bulk SMP with shape memory polymer foam and sheet coatings on the corrugation surface, thicker skins may have a knock-on effect in the overall available volume for fuel and other subsystems within the wingbox.

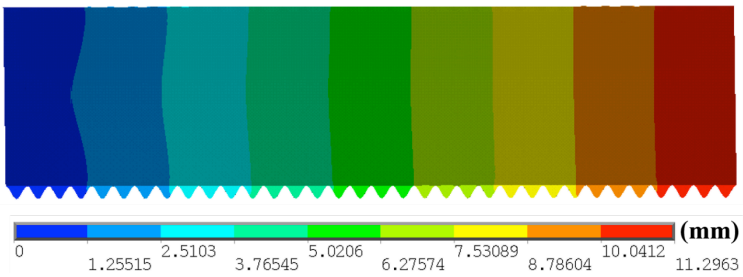

Figure 21. Displacement vector sum on the upper morphing skin for $\alpha=5^{o}$, V=0.3Ma, T=120 ^{o}C, TD=0.1C

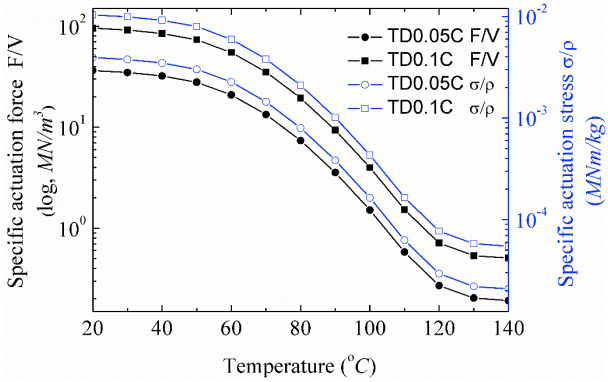

Figure 22 Specific actuation force F/V and stress σ/ρ for different temperature (TD=0.05C and 0.1C)

6 CONCLUSIONS

In this work, a novel variable stiffness corrugated structure for morphing skin application has been designed, modeled and evaluated from an analytical and numerical point of view. The investigation focused on the effects of the unit cell geometrical configurations and the Young's modulus of the SMP matrix to the transverse and bending stiffness of the skin. The theoretical and numerical models show a general good agreement, and they have been applied to evaluate the specific activation stresses and actuation forces per unit volume in a test case representative of an airfoil with continuously variable camber. The novel corrugated structure provides a general smooth external aerodynamic surface, extreme mechanical anisotropic and variable stiffness. While the specific actuation stresses and forces are lower than the ones provided by competitor smart materials and actuation systems, the possibility of local tailoring of the stiffness and large sensitivity with external thermal stimuli make this smart corrugated skin a product amongst the ones to be considered for potential designs of morphing airframe.

Acknowledgements

The support of the FP7-AAT.2012.6.3-1-341509 MORPHELLE and the National Natural Science Foundation of China (Grant No.11225211, 11272106) are gratefully acknowledged. Xiaobo Gong would also like to thank British Council and Chinese Scholarship Council (CSC) for the funding of his research work at the University of Bristol. The Authors also acknowledge the anonymous Reviewers for their useful suggestions and constructive comments.

REFERENCES

[1] Barbarino S, Bilgen O, Ajaj RM, Friswell MI and Inman DJ. A review of morphing aircraft. Journal of Intelligent Material Systems and Structures. 2011;22(9):823-877.
[2] Sofla A, Meguid S, Tan K and Yeo W. Shape morphing of aircraft wing: Status and challenges. Materials & Design. 2010;31(3):1284-1292.
[3] Jha AK and Kudva JN. Morphing aircraft concepts, classifications, and challenges. Proceedings of SPIE - The International Society for Optical Engineering; 2004.
[4] Weisshaar TA. Morphing Aircraft Systems: Historical Perspectives and Future Challenges. Journal of Aircraft. 2007;50(2):337-353.
[5] Armando R. Morphing Aircraft Technology Survey. 45th AIAA Aerospace Sciences Meeting and Exhibit; Reno, Nevada, United States: American Institute of Aeronautics and Astronautics; 2007. 2007-1258.
[6] Thill C, Etches J, Bond I, Potter K and Weaver P. Morphing skins. The Aeronautical Journal. 2008;112(1129):117-139.
[7] Lesieutre GA, Frecker MI, Gandhi FS, Ramrakhyani D, Bharti S, Browne J, et al. Compliant frame: a new paradigm to enable reconfigurable aircraft structures. Air Force Office of Scientific Research, 2007 REPORT No. AFRL-SR-AR-TR-08-0164.
[8] Kudva JN. Overview of the DARPA Smart Wing Project. Journal of Intelligent Material Systems & Structures. 2004;15(4):261-267.
[9] Kudva JN and Sanders BP. Overview of the DARPA/AFRL/NASA Smart Wing program. Proceeding of SPIE-The Industrial and Commercial Applications of Smart Structures Technologies; 1999.
[10] Kudva, J. N, Sanders, B., Pinkertonflorance, J., et al. The DARPA/AFRL/NASA Smart Wing program: Final overview. Proceedings of SPIE-Smart Structures and Materials 2002: Industrial and Commercial Applications of Smart Structures Technologies; 2002.
[11] Kudva JN, Appa K, Way CBV and Lockyer AJ. Adaptive smart wing design for military aircraft: requirements, concepts, and payoffs. Proceeding of SPIE-Smart Structures and Materials 1995: Industrial and Commercial Applications of Smart Structures Technologies; 1995.
[12] Ramrakhyani DS, Lesieutre GA, Frecker MI and Bharti S. Aircraft Structural Morphing using Tendon-Actuated Compliant Cellular Trusses. Journal of Aircraft. 2005;42(6):1614-1620.
[13] Webb LD, Powers SG and Rose LA. Selected Local Flow-Field Measurements on the Advanced Fighter Technology Integration (AFTI)/F-111 Aircraft Mission Adaptive Wing. 1992 REPORT No. NASA-TM-4405.
[14] Dayyani I, Shaw AD, Saavedra Flores EI and Friswell MI. The Mechanics of Composite Corrugated Structures: A Review with Applications in Morphing Aircraft. Composite Structures. 2015:358-380.
[15] Yokozeki T, Takeda S-i, Ogasawara T and Ishikawa T. Mechanical properties of corrugated composites for candidate materials of flexible wing structures. Composites Part A: Applied Science and Manufacturing. 2006;37(10):1578-1586.
[16] Golzar M and Ghabezi P. Corrugated Composite Skins. Mechanics of Composite Materials. 2014;50(2):137-148.
[17] Thill C, Etches J, Bond I, Potter K and Weaver P. Corrugated composite structures for aircraft morphing skin applications. 18th International conference of adaptive structures and technologies, Ottawa, Ontario, Canada 2007.
[18] Yuying X, Rafic MA and Michael IF. Design and Optimisation of Composite Corrugated Skin for a Span Morphing Wing. 22nd AIAA/ASME/AHS Adaptive Structures

Conference; National Harbor, Maryland, United States: American Institute of Aeronautics and Astronautics; 2014. 2014-0762.
[19] Dayyani I, Friswell MI, Khodaparast HH and Woods BKS. The design of a corrugated skin for the FishBAC compliant structure. 22nd AIAA/ASME/AHS Adaptive Structures Conference - SciTech Forum and Exposition, January 13, 2014 - January 17, 2014; National Harbor, MD, United states: American Institute of Aeronautics and Astronautics Inc.; 2014. 2014-1121.
[20] Navaratne R, Dayanni I, Woods BKS and Friswell MI. Development and testing of a corrugated skin for a camber morphing aerofoil. 23nd AIAA/AHS Adaptive Structures Conference 2015, January 5, 2015 - January 9, 2015; Kissimmee, FL, United states: American Institute of Aeronautics and Astronautics Inc.; 2015. 2015-0792.
[21] Dayyani I, Friswell MI, Ziaei-Rad S and Flores EIS. Equivalent models of composite corrugated cores with elastomeric coatings for morphing structures. Composite Structures. 2013;104:281-292.
[22] Dayyani I, Friswell MI and Saavedra Flores EI. A general super element for a curved beam. International Journal of Solids and Structures. 2014;51(17):2931-2939.
[23] Thill C, Etches JA, Bond IP, Potter KD, Weaver PM and Wisnom MR. Investigation of trapezoidal corrugated aramid/epoxy laminates under large tensile displacements transverse to the corrugation direction. Composites Part A Applied Science & Manufacturing. 2010;41(1):168-176.
[24] Ghabezi P and Golzar M. Mechanical analysis of trapezoidal corrugated composite skins. Applied Composite Materials. 2013;20(4):341-353.
[25] Dayyani I, Ziaeirad S and Friswell MI. The mechanical behavior of composite corrugated core coated with elastomer for morphing skins. J Compos Mater. 2014;48(13):1623-1636.
[26] Previtali F, Arrieta AF and Ermanni P. Double-walled corrugated structure for bending-stiff anisotropic morphing skins. Journal of Intelligent Material Systems and Structures. 2015;26(5):599-613.
[27] Previtali F, Molinari G, Arrieta AF, Guillaume M and Ermanni P. Design and experimental characterisation of a morphing wing with enhanced corrugated skin. Journal of Intelligent Material Systems and Structures. 2016;27(2):278-292.
[28] Thill C, Downsborough JD, Lai SJ, Bond IP and Jones DP. Aerodynamic study of corrugated skins for morphing wing applications. Aeronautical Journal. 2010;114(1154):237-244.
[29] Xia Y, Bilgen O and Friswell MI. The effect of corrugated skins on aerodynamic performance. Journal of Intelligent Material Systems and Structures. 2014;25(7):786-794.
[30] Fincham JHS, Ajaj RM and Friswell MI. Aerodynamic performance of corrugated skins for spanwise wing morphing. AIAA AVIATION 2014 -14th AIAA Aviation Technology, Integration, and Operations Conference 2014, June 16, 2014 - June 20, 2014; 2014; Atlanta, GA, United states: American Institute of Aeronautics and Astronautics Inc.
[31] Thill C, Etches JA, Bond IP, Potter KD and Weaver PM. Composite corrugated structures for morphing wing skin applications. Smart Materials and Structures. 2010;19(12):124009.
[32] Dayyani I, Khodaparast HH, Woods BKS and Friswell MI. The design of a coated composite corrugated skin for the camber morphing airfoil. Journal of Intelligent Material Systems and Structures. 2015;26:1592-1608.
[33] Yokozeki T, Sugiura A and Hirano Y. Development of Variable Camber Morphing Airfoil Using Corrugated Structure. Journal of Aircraft. 2014:1-7.

[34] Ursache NM, Melin T, Isikveren AT and Friswell MI. Technology Integration for Active Poly-Morphing Winglets Development. ASME 2008 Conference on Smart Materials, Adaptive Structures and Intelligent Systems; 2008; Ellicott City, Maryland, United States.
[35] Kuder IK, Arrieta AF, Raither WE and Ermanni P. Variable stiffness material and structural concepts for morphing applications. Progress in Aerospace Sciences. 2013;63(0):33-55.
[36] Leng J, Lan X, Liu Y and Du S. Shape-memory polymers and their composites: Stimulus methods and applications. Progress in Materials Science. 2011;56(7):1077-1135.
[37] Gong X, Liu L, Liu Y and Leng J. An electrical-heating and self-sensing shape memory polymer composite incorporated with carbon fiber felt. Smart Materials & Structures. 2016;25(3):035036.
[38] Keihl MM, Bortolin RS, Sanders B, Joshi S and Tidwell Z. Mechanical properties of shape memory polymers for morphing aircraft applications. Proceedings of SPIE - The International Society for Optical Engineering; 2005.
[39] Hemmelgarn CD and Havens E. Adaptive wing structures. Proceedings of SPIE-Smart Structures and Materials 2005: Industrial and Commercial Applications of Smart Structures Technologies; 2005.
[40] Sun J, Liu Y and Leng J. Mechanical properties of shape memory polymer composites enhanced by elastic fibers and their application in variable stiffness morphing skins. Journal of Intelligent Material Systems and Structures. 2015;26(15):2020-2027.
[41] Bye DR and McClure PD. Design of a morphing vehicle. 48th AIAA Structures, Structural Dynamics, and Materials Conference; Honolulu, Hawaii, United States2007. 2007-1728.
[42] McKnight G, Doty R, Keefe A, Herrera G and Henry C. Segmented reinforcement variable stiffness materials for reconfigurable surfaces. Journal of Intelligent Material Systems and Structures. 2010;21(17):1783-1793.
[43] Shimansky RA and Lele MM. Transverse Stiffness of a Sinusoidally Corrugated Plate. Mechanics of Structures & Machines. 1995;23(3):439-451.
[44] El-Sayed FKA, Jones R and Burgess IW. A theoretical approach to the deformation of honeycomb based composite materials. Composites. 1979;10(4):209-214.
[45] Burlayenko VN and Sadowski T. Effective elastic properties of foam-filled honeycomb cores of sandwich panels. Composite Structures. 2010;92(12):2890-2900.
[46] Kingnide O and Farhan G. Modeling and Numerical Analyses of Skin Design Concepts. 50th AIAA/ASME/ASCE/AHS/ASC Structures, Structural Dynamics, and Materials Conference; Palm Springs, California, United States: American Institute of Aeronautics and Astronautics; 2009. 2009-2115.
[47] Jones RM. Mechanics of composite materials: Scripta Book Company Washington, DC; 1975.
[48] Leng J, Wu X and Liu Y. Effect of a linear monomer on the thermomechanical properties of epoxy shape-memory polymer. Smart Materials & Structures. 2009;18(9):7566-7579.
[49] Young WC and Budynas RG. Roark's formulas for stress and strain: McGraw-Hill New York; 2002.
[50] Woods BKS and Friedrich M. Preliminary investigation of a fishbone active camber concept. ASME 2012 Conference on Smart Materials, Adaptive Structures and Intelligent Systems; September 19-21, 2012; Stone Mountain, Georgia, United States2012. SMASIS2012-8058.
[51] Woods BKS, Dayyani I and Friswell MI. Fluid/Structure-Interaction Analysis of the Fish-Bone-Active-Camber Morphing Concept. Journal of Aircraft. 2014:1-13.

[52] Moran J. An introduction to theoretical and computational aerodynamics: Courier Corporation; 1984.
[53] Woods BK, Fincham JH and Friswell MI. Aerodynamic modelling of the fish bone active camber mophing concept. Proceedings of the RAeS Applied Aerodynamics Conference, Bristol, UK; 2014.
[54] Drela M. XFOIL, An Analysis and Design system for Low reynolds Number Airfoils. Conference on Low Reynolds Number Airfoil Aerodynamics, University of Notre Dame; 1989.
[55] Kwok N and Hahn HT. Resistance Heating for Self-healing Composites. J Compos Mater. 2007;41(13):1635-1654.
[56] Jacobs EN. Airfoil section characteristics as affected by protuberances. Langley Memorial Aeronautical Laboratory: National Advisory Committee For Aeronautics, 1932 REPORT No. 446.
[57] Huber JE, Fleck NA and Ashby MF. The selection of mechanical actuators based on performance indices. Proceedings of The Royal Society A: Mathematical, Physical and Engineering Sciences. 1997;453(1965):2185-2205.